Potassium channels contribute to activity-dependent scaling of dendritic inhibition.

Jeremy T. Chang and Michael J. Higley

Department of Neuroscience
Program in Cellular Neuroscience, Neurodegeneration and Repair
Kavli Institute
Yale School of Medicine
New Haven, CT 06510

Correspondence: m.higley@yale.edu

Abstract

GABAergic inhibition plays a critical role in the regulation of neuronal activity. In the neocortex, inhibitory interneurons that target the dendrites of pyramidal cells influence both electrical and biochemical postsynaptic signaling. Voltage-gated ion channels strongly shape dendritic excitability and the integration of excitatory inputs, but their contribution to GABAergic signaling is less well understood. Here, we examine the actions of potassium channels in regulating dendritic inhibition in mouse visual cortex. By combining 2-photon calcium imaging and focal GABA uncaging, we show that A-type channels normally suppress the GABAergic inhibition of calcium signals evoked by back-propagating action potentials in dendritic spines and shafts. Moreover, the voltage-dependent inactivation of these channels leads to enhancement of dendritic inhibition following somatic spiking. Overall, our findings highlight the interaction between intrinsic and synaptic properties and reveal a novel mechanism for the activity-dependent scaling of GABAergic inhibition.

Introduction

Inhibition in the neocortex is primarily mediated by the neurotransmitter gamma-aminobutyric acid (GABA) through synaptic contacts made by interneurons. These synapses are distributed across the entire somatodendritic arbor and work to counteract excitatory glutamatergic input. GABAergic synapses that target the axon initial segment and soma exert a strong influence on somatic voltage, and consequently play important roles in regulating the generation and timing of action potentials (Higley and Contreras, 2006; Pouille and Scanziani, 2001; Wehr and Zador, 2003; Zhu et al., 2004). However, the vast majority of inhibitory inputs are formed onto pyramidal cell dendrites (Beaulieu and Somogyi, 1990), and the role of dendrite-targeting inhibition has been an area of growing interest (Bloss et al., 2016; Lovett-Barron et al., 2012; Miles et al., 1996). One important function of dendritic inhibition, in addition to action potential regulation, is the regulation of dendritic calcium signals which are thought to play an instructive role in synaptic plasticity (Chiu et al., 2013; Palmer et al., 2012; Tsubokawa and Ross, 1996). Recent reports in the neocortex and hippocampus have described varying efficacy of dendritic calcium inhibition, ranging from spatial compartmentalization within individual spines to complete abolition of actively propagating action potentials (Chiu et al., 2013; Kanemoto et al., 2011; Marlin and Carter, 2014; Mullner et al., 2015; Stokes et al., 2014). The mechanisms underlying this heterogeneity are unclear, but one contributing factor may be variations in intrinsic dendritic properties, like voltage-dependent channels, whose impact on GABAergic inhibition is not well understood.

The expression of voltage-gated ion channels within neuronal dendrites regulates cellular excitability and strongly influences synaptic integration (Cook and Johnston, 1999; Johnston and Narayanan, 2008; Miller et al., 1985; Poirazi and Mel, 2001; Shepherd et al., 1985). One example is the A-type potassium (KA) conductance, characterized by fast inactivation and sensitivity to 4-aminopyridine (4-AP)(Bekkers, 2000; Clark et al., 2008; Korngreen and Sakmann, 2000; Serodio and Rudy, 1998). Within cortical and hippocampal pyramidal neurons, KA channels are expressed throughout the dendritic arbor and have been implicated in the regulation of back-propagating action potentials (bAPs) and excitatory synaptic integration (Cai et al., 2004; Carrasquillo et al., 2012; Gasparini, 2011; Harnett et al., 2013; Hoffman et al., 1997; Ramakers and Storm, 2002). Despite clearly influencing dendritic excitation, KA channels have been shown to preferentially co-localize with GABAergic synapses, suggesting they may also play a role in the control of inhibition (Burkhalter et al., 2006; Jinno et al., 2005).

Here, we examine how voltage-gated potassium channels alter GABAergic inhibition of bAP-evoked Ca2+ signals (ΔCa2+) in dendrites of L5 pyramidal neurons in mouse visual cortex. We show that the blockade of these channels specifically in the apical dendrite enhances both the amplitude and inhibition of bAP-evoked ΔCa2+. Moreover, our data suggest the involvement of dendritic Kv4 channels, previously shown to play a role in dendritic excitability. We also show that the voltage-dependent inactivation of these channels gives rise to a scaling of dendritic GABAergic inhibition, such that inhibitory efficacy is enhanced following strong somatic activity. Thus, our findings demonstrate that intrinsic excitability interacts with GABAergic synaptic input to dynamically regulate dendritic Ca2+ signaling.

69

70 **Results**

71 In order to investigate the impact of potassium channels on dendritic inhibition, we performed
72 two-photon calcium imaging of bAP-evoked dendritic Ca2+ transients in layer 5 pyramidal neurons
73 (L5PNs) of mouse visual cortex (Figure 1A). Ca2+ signals were measured in dendritic spines and
74 neighboring shafts along the primary apical dendrite, 100-150 μm from the soma (Figure 1B). To probe
75 the effects of GABAergic inhibition on ΔCa2+, we compared uninhibited ΔCa2+ from bAPs induced by
76 somatic current injection with ΔCa2+ from bAPs preceded (15 ms) by local (at the imaging site) uncaging
77 of RuBi-GABA (Rial Verde et al., 2008). To compare observations across different recordings, GABAergic
78 inhibition of ΔCa2+ was quantified as in previous studies as $(\Delta Ca2+_{Ctl}-\Delta Ca2+_{Inh})/\Delta Ca2+_{Ctl}$ (Chiu et al.,
79 2013). The magnitude of this Ca2+ inhibition was measured before and after bath-application of the
80 potassium channel blocker 4-aminopyridine (4-AP)(Figure 1A). Treatment with 4-AP broadened the
81 somatic action potential (p=0.0020)(Figure 1C) and increased the average peak ΔCa2+ evoked by a
82 single bAP for both spines (p=0.0059) and neighboring shafts (p=0.0137) (Figure 1D-G). Moreover, 4-AP
83 significantly enhanced the average GABAergic inhibition of ΔCa2+ for both spines (p=0.0195) and
84 neighboring shafts (p=0.0098) (Figure 1D-G). Importantly, this result was not seen when slices were pre-
85 treated with the $GABA_AR$ antagonist picrotoxin (Figure 1 - figure supplement 1) nor with application of
86 control saline, which demonstrated the presence of a run-down in peak ΔCa2+ over time without change
87 in Ca2+ inhibition (Figure 1 - figure supplement 2), consistent with previous findings (Canepari et al.,
88 2007; Chalifoux and Carter, 2011; Fukumoto et al., 2012; Kameyama et al., 1989).

89 Given the enhanced GABAergic inhibition of dendritic ΔCa2+ following 4-AP treatment, we next
90 asked whether 4-AP also altered the somatic inhibitory postsynaptic potential (IPSP) evoked by
91 GABAergic dendritic input. We analyzed IPSPs evoked by either single uncaging events or bursts of three
92 uncaging events (10 Hz), directed to the proximal apical dendrite as above. In the presence of 4-AP,
93 IPSP amplitude was enhanced for both single (p=0.0391) and triple (p=0.0039) uncaging protocols
94 (Figure 1— figure supplement 3A-C). Concurrent with the increase in IPSP amplitude, the decay of the
95 IPSP was also significantly slowed after treatment with 4-AP (p=0.0039), leading to enhanced temporal
96 summation for bursts of IPSPs (Figure 1—figure supplement 3C-D). The IPSP alterations could be
97 explained by a significant increase in somatic input resistance measured using a series of negative
98 current steps (p=0.0391)(Figure 1—figure supplement 3E). In sum, these data suggest voltage-
99 dependent potassium channels normally suppress the somatic and dendritic effects of GABAergic
100 inhibition in the apical dendrite.

101 Next, we asked whether the actions of 4-AP-sensitive channels on inhibition of dendritic ΔCa2+
102 generalized to other subcellular regions, as previous reports have suggested differential contributions to
103 excitability in basal and apical dendrites (Sandler et al., 2016). We performed similar imaging experiments
104 in basal dendrites (100-150 µm from the soma) (Figure 1—figure supplement 4A-D). Again, the bAP-
105 evoked ΔCa2+ was significantly increased by 4-AP for both spines (p= 0.0026) and neighboring shafts

106 (p= 0.0020). However, GABAergic inhibition of ΔCa2+ was much stronger in the basal dendrites and was
107 not further enhanced by application of 4-AP for either spines (p= 0.1602) or neighboring shafts (p=
108 0.2754) (Figure 1—figure supplement 3B-D). Note that while the fractional inhibition of ΔCa2+ was not
109 altered, the absolute inhibition of ΔCa2+ influx was enhanced by 4-AP. Thus, our results suggest that
110 potassium channels differentially shape GABAergic efficacy in apical versus basal dendrites.

111 As bath application of 4-AP altered both somatic and apical dendritic effects of GABAergic
112 inhibition, we investigated whether these actions arise from similar or distinct pools of potassium
113 channels. We used a puffer pipette to locally apply 4-AP at different locations along the somatodendritic
114 axis. When applied to the proximal apical dendrite (at the site of GABA uncaging), 4-AP replicated the
115 effects of bath-application on the magnitude of bAP-evoked ΔCa2+ and its inhibition by GABA.
116 Specifically, 4-AP increased ΔCa2+ in spines (p=0.0156) and neighboring shafts (p=0.0313) (Figure 2A-
117 D). GABAergic inhibition of ΔCa2+ was also enhanced in spines (p=0.0469) and neighboring shafts
118 (p=0.0313) (Figure 2A-D). In contrast, application of 4-AP to either the cell body or apical tuft had no
119 impact on peak ΔCa2+ or its inhibition by GABA within the proximal apical dendrite (Figure 2— figure
120 supplement 1A-G). Conversely, the effects of bath-applied 4-AP on somatic IPSPs evoked by dendritic
121 GABA uncaging were mimicked by focal application to the soma but not the proximal apical dendrite
122 (Figure 2— figure supplement 2). Thus, our data suggest that the somatic and dendritic impacts of
123 dendritic GABAergic inhibition are modulated by two spatially separated pools of potassium channels.

124 While 4-AP-sensitive potassium currents can be mediated by a variety of molecularly-defined
125 channels, A-type Kv4.2 channels have been specifically linked to the control of dendritic excitability
126 (Carrasquillo et al., 2012; Harnett et al., 2013; Losonczy et al., 2008; Sandler et al., 2016). We therefore
127 investigated the contribution of these channels to the regulation of GABAergic inhibition using the
128 scorpion toxin AmmTx3, which specifically blocks Kv4.2 and Kv4.3 channels in the presence of the
129 auxiliary subunit dipeptidyl-peptidaselike-protein 6 (DPP6) (Maffie et al., 2013). Similar to our results with
130 4-AP, GABAergic inhibition of bAP-evoked ΔCa2+ was significantly enhanced following bath application
131 of 200 nM AmmTx3 for both spines (p=0.0195) and neighboring shafts (p=0.0488) (Figure 3A-D).
132 Following AmmTx3 application, there was no change in the amplitude of the bAP-evoked ΔCa2+ in spines
133 (p=0.3223) and ΔCa2+ was significantly reduced in dendritic shafts (p=0.0137) relative to baseline (Figure
134 3B-D). However, the observation that ΔCa2+ exhibits considerable run-down over time (see Figure 1 -
135 figure supplement 2) suggests that AmmTx3 likely produces a small enhancement of bAP-evoked ΔCa2+
136 relative to control conditions that is masked by the run-down. Consistent with previous studies (Pathak et
137 al., 2016), AmmTx3 had no effect on either somatic input resistance or IPSP amplitude (Figure 3— figure
138 supplement 1).

139 As the effects of AmmTx3 application did not completely recapture those of 4-AP, we quantified
140 the contribution of Kv4 channels to L5PN membrane currents by recording from somatic outside-out
141 macropatches. Application of 4-AP blocked a fast outward current by -73.5 ± 6.8%. In contrast,
142 application of AmmTx3 produced a significantly smaller -43.1 ± 11.2% change in current (p=0.0417,

143 unpaired t-test), demonstrating that Kv4 channels sensitive to AmmTx3 constitute a fraction of the
144 voltage-gated potassium channels blocked by 4-AP in L5PNs (Figure 3 - figure supplement 2). Altogether,
145 these results suggest that the activity of A-type Kv4 channels is sufficient to influence dendritic Ca2+
146 signaling and GABAergic inhibition.

147 One notable feature of KA channels is their fast, voltage-dependent inactivation, which limits their
148 conductance during periods of high neuronal activity (Bekkers, 2000; Kim et al., 2005). We therefore
149 asked whether KA channels might enable dendritic GABAergic inhibition to dynamically scale with
150 somatic firing. To test this hypothesis, we compared GABAergic inhibition of ΔCa2+ evoked by a bAP
151 alone or preceded 20 ms by a train of 5 bAPs at 100 Hz (Figure 4A). Similar to 4-AP, the preceding train
152 significantly enhanced the peak ΔCa2+ for both spines (p= 0.002) and neighboring shafts (p= 0.002) and
153 also enhanced GABAergic inhibition of ΔCa2+ for spines (p=0.0059) and neighboring shafts (p= 0.002)
154 (Figure 4B-D). In contrast, preceding spike trains at 50 Hz had minimal effect on either ΔCa2+ amplitude
155 or GABAergic inhibition (Figure 4— figure supplement1A-D). Importantly, the ability of the 100 Hz train to
156 enhance dendritic inhibition was occluded by prior bath application of 4-AP, suggesting that KA channels
157 are required for activity-dependent scaling (Figure 4— figure supplement 1E-H).

158 We next asked whether activity-dependent scaling of inhibition could be seen with synaptic GABA
159 release. To test this, we expressed channelrhodopsin-2 (ChR2) in a subset of dendrite-targeting cortical
160 interneurons expressing somatostatin (SOM-INs)(Figure 5A). Brief pulses of blue light were used to
161 activate SOM-INs and produce postsynaptic IPSPs. We repeated experiments comparing the GABAergic
162 inhibition of ΔCa2+ evoked by a bAP alone or preceded by a 100 Hz train. As with GABA uncaging, trains
163 of somatic action potentials significantly enhanced the magnitude of ΔCa2+ in spines (p=0.0098) and
164 neighboring shafts p=0.0059) and led to stronger GABAergic inhibition of ΔCa2+ for both spines
165 (p=0.0273) and neighboring shafts (p=0.0273) (Figure 5B-D). Taken together, these results demonstrate
166 that KA channels in the apical dendrite play a key role in reducing the impact of synaptic GABAergic
167 inhibition on bAP-evoked ΔCa2+.

168 Finally, to examine the biophysical mechanisms underlying the interaction of dendritic potassium
169 channels with GABAergic signaling, we simulated an active dendritic compartment and tested the impact
170 of varying voltage-gated conductances on the magnitude of Ca2+ inhibition (Figure 6). We first explored
171 whether increased GABAergic inhibition was mediated by 4-AP-induced enhancement of dendritic
172 depolarization and the resulting increase in chloride driving force. The model revealed the surprising
173 finding that increasing bAP-dependent depolarization by increasing the sodium reversal potential actually
174 reduced GABAergic inhibition (Figure 6A-B). In contrast, reducing KA channel conductance recapitulated
175 our data, increasing both bAP amplitude and the amount of Ca2+ current inhibited by GABAergic
176 signaling (Figure 6A-C). Thus, alterations in peak depolarization attained during the bAP alone do not
177 account for the enhanced Ca2+ inhibition (Figure 6D). Instead, we found that manipulations that
178 increased the bAP duration (e.g., decreasing either E_{Na} or g_A) led to increased Ca2+ inhibition (Figure
179 6E). This phenomenon is illustrated in Figure 6A, where similar inhibition of the bAP peak leads to greater

reduction in the integrated Ca2+ current (yellow shaded areas) for broader bAP waveforms. In summary, these observations strongly suggest that the contribution of potassium conductance to bAP duration is an important factor in the magnitude of Ca2+ inhibition.

Discussion

Rapidly activating and inactivating A-type potassium channels are widely recognized as key modulators of neuronal excitability as well as synaptic integration and plasticity (Carrasquillo et al., 2012; Foeger et al., 2012; Harnett et al., 2013; Hoffman et al., 1997; Losonczy et al., 2008; Magee and Carruth, 1999). In the present work, we have described a role for KA channels in the regulation of dendritic GABAergic inhibition and its control over dendritic Ca2+ signaling. Using a combination of electrophysiology, 2-photon Ca2+ imaging, and focal GABA uncaging, we show that blocking KA channels either pharmacologically or via activity-dependent inactivation enhances both bAP-evoked Ca2+ influx and GABAergic inhibition of these transients in the apical dendrites of L5PNs. Moreover, this modulation of dendritic signaling can occur in the absence of changes to the somatically recorded IPSP. These results provide evidence that KA channels compartmentalize their regulation of GABAergic signaling.

Dendritic potassium channels comprise a diverse molecular group, including both Kv1-, Kv3, and Kv4-type channels (Carrasquillo et al., 2012; Serodio et al., 1994). Our pharmacological analysis indicates a contribution from Kv4 channels, previously shown to be expressed in both cortical and hippocampal pyramidal dendrites. Indeed the ability of AmmTx3 to replicate the actions of 4-AP on GABAergic Ca2+ inhibition suggests that Kv4 channels in L5PNs include the auxiliary subunit dipeptidyl-peptidase-like-protein 6 (DPP6), in agreement with previous studies (Foeger et al., 2012; Pathak et al., 2016). Nevertheless, AmmTx3 produces a smaller change in inhibition compared with 4-AP, suggesting that other voltage-gated potassium channels also play a role in regulating dendritic GABAergic signaling. This conclusion is supported by our data from outside-out somatic patches. Notably, the expression of Kv4.2 channels is regulated by the activity of NMDA-type glutamate receptors, indicating the possibility for multiple feedback loops within pyramidal neuron dendrites (Kim et al., 2007; Sandler et al., 2016).

Several previous studies have implicated KA channels in the regulation of both dendritic excitability and glutamatergic synaptic integration. In both CA1 and cortical pyramidal neurons, the presence of KA channels limits the spread of voltage between distinct compartments, such as the distal and proximal apical dendrite, regulating both the back propagation of action potentials and the spread of synaptically evoked dendritic spikes (Cai et al., 2004; Frick et al., 2003; Harnett et al., 2013; Kim et al., 2007; Kim et al., 2005; Losonczy et al., 2008). Our study demonstrates that KA channels similarly restrict the efficacy of GABAergic inhibition, suggesting that KA channels generally serve as dendritic “shock absorbers”, limiting the impact of synaptic inputs from all sources (Yuste, 1997). An intriguing possibility is that voltage-gated potassium channels asymmetrically regulate excitation and inhibition, potentially leading to moment-to-moment alterations of the balance between these opposing drives. Disruption of the

217 normal balance of excitatory and inhibitory signaling is thought to occur in a number of neuropsychiatric
218 disorders, including autism and schizophrenia. Indeed, in Fragile X syndrome, loss of FMRP produces a
219 dysregulation of KA channels that could lead to an imbalance of excitation and inhibition (Brager and
220 Johnston, 2014; Gross et al., 2011; Kalmbach et al., 2015). Future studies are necessary to elucidate the
221 precise role of KA channels in shaping glutamatergic and GABAergic integration.

222 In addition to regulating dendritic excitability, KA channels have been implicated in shaping long-
223 term plasticity of glutamatergic synapses. In particular, studies have focused on spike-timing dependent
224 plasticity (STDP), where bAPs can potentiate or depress synaptic inputs depending on their relative
225 timing to synaptic activity (Magee and Johnston, 1997; Markram et al., 1997). For example, EPSPs in
226 CA1 pyramidal neuron dendrites can inactivate KA channels, enhancing the dendritic invasion of somatic
227 action potentials and subsequent plasticity (Hoffman et al., 1997). Recent experimental and
228 computational studies have also suggested a key role for GABAergic inhibition in spike-timing dependent
229 plasticity (Cichon and Gan, 2015; Hayama et al., 2013; Paille et al., 2013; Wilmes et al., 2016). For
230 example, focal activation of GABAergic synapses in CA1 dendrites was shown to convert long-term
231 potentiation to depression due to negative regulation of dendritic Ca2+ influx (Hayama et al., 2013).
232 Together, these various findings suggest that the interaction of NMDARs, KA channels, and GABAergic
233 inhibition may strongly contribute to the development and maintenance of cortical circuits.

234 It is intriguing to speculate that expression patterns of KA channels may also explain some of the
235 recent diversity in studies examining GABAergic control of dendritic ΔCa2+. Previous work from our lab
236 showed that inhibition could be highly compartmentalized in layer 2/3 pyramidal neurons, with
237 neighboring spines exhibiting markedly different amounts of inhibition (Chiu et al., 2013). In contrast, work
238 from other groups has shown that more broad dendritic inhibition can occur in L5PNs and hippocampal
239 CA1 pyramidal neurons (Marlin and Carter, 2014; Mullner et al., 2015; Stokes et al., 2014). Differential
240 expression and recruitment of voltage-gated conductances, such as KA channels, would be expected to
241 contribute to the heterogeneity of inhibitory function across cell types.

242 Our computational modeling provides additional insight into the biophysical mechanism
243 underlying the interaction of KA channels and GABAergic inhibition. We found that decreasing the
244 potassium conductance, rather than increasing the bAP amplitude per se, was necessary to enhance
245 dendritic Ca2+ inhibition. This phenomenon is directly due to the broadening of the bAP duration and
246 subsequent reduction in the integral Ca2+ current (see Figure 6A). This finding suggests that a major
247 contributor to the efficacy of GABAergic regulation of action potentials is the relationship between bAP
248 duration and Ca2+ current. In addition, our computational modeling suggests that the enhancement of
249 GABAergic inhibition is a general biophysical feature of channels that broaden action potentials. AP width
250 has been linked to the coupling of AP into dendrites and dendritic location (Golding et al., 2001; Stuart et
251 al., 1997). Furthermore KA channels have been linked to both activity dependent as well as cell type
252 dependent alteration of action potential repolarization (Kim et al., 2005; Pathak et al., 2016). Our model
253 and experimental findings together thus predict that dendritic channels that regulate bAP shape are likely

to be important factors in altering the dendritic influence of GABAergic synapses, driving cell type- and subcellular location-dependent differences in the efficacy of GABAergic inhibition.

Finally, we found that the voltage-dependent inactivation of KA channels allows for the enhancement of GABAergic inhibition in the presence of high frequency somatic spike generation. This suggests that dendritic inhibition may exert greater control over Ca2+ signaling during periods of high network activity or somatic depolarization, essentially acting as a source of homeostatic control. These findings are consistent with previous experimental and computational studies demonstrating the activity-dependent amplification of trains of bAPs and bAP width in L5PN apical dendrites (Grewe et al., 2010; Kim et al., 2005; Larkum et al., 1999). Our results suggest that the dynamic properties of active dendritic conductances such as KA channels enable the alteration of GABAergic inhibition over short millisecond time frames, providing the basis for a context-dependent, flexible role of GABAergic signaling in shaping biochemical and electrical signaling in dendrites.

Materials and Methods

Slice Preparation

All animal handling was performed in accordance with guidelines approved by the Yale Institutional Animal Care and Use Committee and federal guidelines. For GABA uncaging experiments, subjects were male wild-type C57-BL6 mice, ages P30-40 (Harlan). For optogenetic experiments, subjects were male and female SOM-Cre mice, ages P30-40 (IMSR Cat# JAX:013044, RRID:IMSR_JAX:013044). Under isofluorane anesthesia, mice were decapitated and coronal slices (300 μm thick) containing primary visual cortex were cut in ice cold external solution containing (in mM): 110 choline, 25 NaHCO3, 1.25 NaH2PO4, 2.5 KCl, 7 MgCl2, 0.5 CaCl2, 20 glucose, 11.6 sodium ascorbate, and 3.1 sodium pyruvate, bubbled with 95% O2 and 5% CO2. After an incubation period of 20 minutes at 34°C, slices were transferred to artificial cerebrospinal fluid (ACSF) containing in (mM): 127 NaCl, 25 NaHCO3, 1.25 NaH2PO4, 2.5 KCl, 1 MgCl2, 2 CaCl2, and 20 glucose bubbled with 95% O2 and 5% CO2 and maintained at room temperature (20-22°C) for at least 20 min until use.

Electrophysiology and imaging

Experiments were conducted at room temperature in a submersion type recording chamber. Whole-cell patch clamp recordings were obtained from layer 5 pyramidal neurons (500 µm to 600 µm from the pial surface) identified with video infrared-differential interference contrast. For current-clamp recordings, glass electrodes (2-4 MΩ tip resistance) were filled with internal solution containing (in mM): 135 KMeSO3, 10 HEPES, 4 MGCl2, 4 Na2ATP, 0.5 NaGTP, and 10 sodium creatine phosphate, adjusted to pH 7.3 with KOH. For Ca2+ imaging experiments, red fluorescent Alexa Fluor-568 (40 μM) and green fluorescent Ca2+-sensitive Fluo-5F (300 μM) were included in the pipette solution to visualize cell morphology and changes of intracellular Ca2+ concentration, respectively. In experiments where only

291 somatic IPSPs or outside-out patches were recorded, Alexa Fluor-568 (40 μM) and EGTA (100 μM) were
292 included in the internal solution. Electrophysiological recordings were made using a Multiclamp 700B
293 amplifier (Molecular Devices), filtered at 4 kHz, and digitized at 10 kHz. For all recordings, membrane
294 potential was adjusted to -64 mV using current injection through the pipette. Steady state somatic chord
295 input resistance was determined by linearly fitting the amplitude of response to 600 ms current injections
296 of -300, -200, and -100 pA.

297 Outside-out macropatch data was obtained in voltage clamp configuration. Patches were formed
298 after whole-cell configuration was obtained by withdrawing the pipet without additional suction. Holding
299 potential was maintained at -75 mV. After a 1 s voltage step to -90 mV, voltage dependent membrane
300 currents were recorded in response to a 500 ms voltage step to +35 mV. Passive leak was removed
301 using a P/N subtraction method of the response from -110 mV to -140 mV. A-type currents were
302 quantified over a 50 ms window beginning 5 ms after the depolarizing voltage step to avoid stimulus
303 artifact.

304 Two-photon imaging was performed with a custom-modified Olympus BX51-WI microscope,
305 including components manufactured by Mike's Machine Company. Fluorophores were excited using 840
306 nm light from a pulsed titanium-sapphire laser. Emissions were separated using appropriate optical filters
307 (Chroma, Semrock) and collected by photomultiplier tubes (Hamamatsu). A mechanical shutter was
308 placed in front of the collectors to prevent damage during blue light stimulation. For Ca2+ imaging, signals
309 were collected during a 500 Hz line scan across a spine and neighboring dendritic shaft on the main
310 apical trunk 100 µm to 150 µm from the cell body. Back-propagating action potentials (bAPs) were
311 evoked using a brief depolarizing current pulse (0.5 ms, 1.5-2.5 nA) through the recording pipette. Trials
312 including bAP alone, IPSP-bAP, and IPSP alone were interleaved with a 45 second inter-trial interval. In a
313 subset of experiments, trains of action potentials at 50 Hz and 100 Hz were elicited by current pulse
314 injections through the recording pipette, ending 20 ms prior to a single current pulse. In this case, trials
315 including single bAP alone, train-bAP alone, IPSP-bAP, train-IPSP-bAP, IPSP alone, train-IPSP, and train
316 alone were interleaved with a 45 ms inter-trial interval. Fluorescent traces were computed for individual
317 cells as the average of 10 trials.

318 Reference frame scans were taken between each acquisition to correct for small spatial drift over
319 time. Ca2+ signals were first quantified as changes in green fluorescence from baseline normalized to the
320 average red fluorescence (ΔG/R). To permit comparison of the imaging data across various microscope
321 configurations, we expressed fluorescence changes as the fraction of the G/R ratio measured in
322 saturating Ca2+ (ΔG/Gsat).

323

324 **Data acquisition and analysis**

325 Imaging and physiology data were acquired using custom software written in MATLAB. Off-line
326 analysis was performed using custom routines written in MATLAB (MATLAB, RRID:SCR_001622) and
327 IgorPro (Wavemetrics Software, RRID:SCR_000325). Ca2+ responses were calculated as the integral of

328 the fluorescence transient over the first 100 ms after bAP initiation. In order to enable comparisons across
329 cells, Ca2+ inhibition was expressed as in previous studies (Chiu et al., 2013) as ($\Delta Ca2+_{Ctl}$-
330 $\Delta Ca2+_{Inh}$)/$\Delta Ca2+_{Ctl}$. IPSPs were computed as the average of 10 trials, and amplitudes were calculated by
331 finding the peak of the voltage trace and averaging values across a surrounding 3 ms window. IPSP
332 decay kinetics were calculated by fitting an exponential to the falling phase of the IPSP. All statistical
333 comparisons were made using the non-parametric Wilcoxon matched pairs signed rank test in GraphPad
334 Prism version 7.01 (GraphPad Prism, RRID:SCR_002798) unless otherwise noted.
335
336 **Pharmacology**
337 For all GABA uncaging experiments, ACSF included 3 μM CGP-55845 hydrochloride (Tocris Cat.
338 No. 1248) to block GABAB receptors, 10 μM (R)-CPP (Tocris Cat. No. 0247) to block NMDA receptors,
339 and 10 μM NBQX disodium salt (Tocris Cat. No. 1044) to block AMPA receptors. For a subset of
340 experiments, the ACSF included 5 mM 4-aminopyradine (Tocris Cat. No. 0940), 200 nM AmmTx3
341 (Smartox Biotechnology), or 100 μM picrotoxin (Tocris Cat. No 1128). Outside-out potassium currents
342 were recorded in the presence of 1 μM tetrodotoxin (Tocris Ca. No 1078). Local application of 25 mM 4-
343 AP was achieved using a glass puffer pipette (< 2 μm tip) coupled to a Picospritzer. Drugs were ejected
344 continuously with 10-17 psi, and pipettes were position 30-70 μm from the targeted structure at the
345 surface of the slice. In experiments where one-photon uncaging was performed with local drug
346 application, 10.8 μM RuBi-GABA was included in the puffer pipette. In a subset of cells, somatic current
347 injections elicited bursts of action potentials in the presence of 4-AP and were excluded from subsequent
348 analysis.
349 Visible light-evoked GABA uncaging was accomplished using RuBi-GABA (10.8 μM) bath-
350 applied in the ACSF(Rial Verde et al., 2008). We overfilled the back aperture of the microscope objective
351 (60x, 1.0 NA) with collimated blue light from a fiber-coupled 473 nm laser. Spherical aberrations due to
352 fiber-coupling resulted in a 15-20 μm diameter disc of light at the focal plane centered on the field of view.
353 A brief (0.5 ms) pulse of light (1-2 mW at the sample) reliably evoked uncaging-evoked IPSPs. For Ca2+
354 imaging experiments, a blue light photo-artifact was corrected by subtracting fluorescence traces on
355 uncaging-alone trials from those with Ca2+ imaging. For all experiments, GABA uncaging occurred 15 ms
356 prior to bAP initiation.
357
358 **ChR2 Expression and Activation**
359 To stimulate SOM-INs, SOM-Cre mice were injected 13-23 days prior to slice preparation into the
360 primary visual cortex with recombinant adeno-associated virus (AAV) driving conditional expression of a
361 ChR2-eYFP fusion protein under the Ef1a-promoter (AAV-DIO-Ef1a-ChR2-EYFP)(UNC Vector Core).
362 Optogenetic stimulation was accomplished using the same light source and path as one-photon GABA
363 uncaging (see above). Brief (2-3 mW, 0.5 ms) pulses were used to stimulate SOM-INs 15 ms prior to bAP
364 initiation.

365

366 **NEURON Modeling**

367 Multi-compartment time-dependent simulations were run using NEURON v7.4 (NEURON,
368 RRID:SCR_005393, available free at http://neuron.med.yale.edu) and analyzed using custom scripts
369 written in Jupyter Notebooks 4.1.0 using Python 3.5.2. We modified a previously published ball and stick
370 model (Chiu et al., 2013) adding compartments for a basal dendrite and two apical tuft dendrites. A single
371 dendritic spine (1 μm diameter) was attached to the apical dendrite 122.5 μm from the cell body by a neck
372 (1 μm length, 0.07 μm diameter). A medium voltage-gated calcium channel was inserted into the dendritic
373 spine and neighboring dendrite such that currents through these channels would minimally impact
374 membrane potential (Almog and Korngreen, 2014). GABAergic synapses were modeled as an
375 exponential synapse contacting the dendritic shaft located 123.5 μm from the cell body. We modeled KA
376 currents using a previously published channel definition that fits observed A-type potassium currents in
377 distal dendrites and altered the expression pattern of this channel and sodium currents in the apical
378 dendrite (Acker and Antic, 2009; Migliore et al., 1999). In order to reproduce our experimental conditions,
379 an iterative search was conducted to find a somatic current injection that maintained the somatic resting
380 potential at 64.00 +/- 0.0001 mV at the cell body for each condition tested. Similar to our experiments we
381 quantified calcium flux over a 100 ms window in order to calculate percent calcium change due to
382 inhibition. To speed up simulation time, simulations were run in parallel using the built-in message
383 passing interface of NEURON.

384

385

386 **Acknowledgements**

387 The authors thank Drs. Jess Cardin, Susumu Tomita, and Michael Crair as well as members of the Higley
388 lab for constructive comments during the preparation of this manuscript. Experiments were supported by
389 funding from the March of Dimes (Basil O'Connor Award) and the NIH (R01 MH099045, T32 EY22312).

390

391

392 **References**

393

394 Acker, C.D., and Antic, S.D. (2009). Quantitative assessment of the distributions of membrane
395 conductances involved in action potential backpropagation along basal dendrites. J Neurophysiol
396 *101*, 1524-1541. doi:10.1152/jn.00651.2007
397 Almog, M., and Korngreen, A. (2014). A quantitative description of dendritic conductances and its
398 application to dendritic excitation in layer 5 pyramidal neurons. J Neurosci *34*, 182-196.
399 doi:10.1523/JNEUROSCI.2896-13.2014
400 Beaulieu, C., and Somogyi, P. (1990). Targets and Quantitative Distribution of GABAergic Synapses in
401 the Visual Cortex of the Cat. Eur J Neurosci *2*, 896. doi:10.1111/j.1460-9568.1990.tb00421.x
402 Bekkers, J.M. (2000). Distribution and activation of voltage-gated potassium channels in cell-attached and
403 outside-out patches from large layer 5 cortical pyramidal neurons of the rat. J Physiol *525 Pt 3*, 611-
404 620. doi:10.1111/j.1469-7793.2000.t01-2-00611.x
405 Bloss, E.B., Cembrowski, M.S., Karsh, B., Colonell, J., Fetter, R.D., and Spruston, N. (2016). Structured
406 Dendritic Inhibition Supports Branch-Selective Integration in CA1 Pyramidal Cells. Neuron *89*, 1016-
407 1030. doi:10.1016/j.neuron.2016.01.029
408 Brager, D.H., and Johnston, D. (2014). Channelopathies and dendritic dysfunction in fragile X syndrome.
409 Brain Res Bull *103*, 11-17. doi:10.1016/j.brainresbull.2014.01.002
410 Burkhalter, A., Gonchar, Y., Mellor, R.L., and Nerbonne, J.M. (2006). Differential expression of I(A)
411 channel subunits Kv4.2 and Kv4.3 in mouse visual cortical neurons and synapses. J Neurosci *26*,
412 12274-12282. doi:10.1523/JNEUROSCI.2599-06.2006
413 Cai, X., Liang, C.W., Muralidharan, S., Kao, J.P., Tang, C.M., and Thompson, S.M. (2004). Unique roles
414 of SK and Kv4.2 potassium channels in dendritic integration. Neuron *44*, 351-364.
415 doi:10.1016/j.neuron.2004.09.026
416 Canepari, M., Djurisic, M., and Zecevic, D. (2007). Dendritic signals from rat hippocampal CA1 pyramidal
417 neurons during coincident pre- and post-synaptic activity: a combined voltage- and calcium-imaging
418 study. J Physiol *580*, 463-484. doi:10.1113/jphysiol.2006.125005
419 Carrasquillo, Y., Burkhalter, A., and Nerbonne, J.M. (2012). A-type K+ channels encoded by Kv4.2, Kv4.3
420 and Kv1.4 differentially regulate intrinsic excitability of cortical pyramidal neurons. J Physiol *590*,
421 3877-3890. doi:10.1113/jphysiol.2012.229013
422 Chalifoux, J.R., and Carter, A.G. (2011). GABAB receptor modulation of voltage-sensitive calcium
423 channels in spines and dendrites. J Neurosci *31*, 4221-4232. doi:10.1523/JNEUROSCI.4561-10.2011
424 Chiu, C.Q., Lur, G., Morse, T.M., Carnevale, N.T., Ellis-Davies, G.C., and Higley, M.J. (2013).
425 Compartmentalization of GABAergic inhibition by dendritic spines. Science *340*, 759-762.
426 doi:10.1126/science.1234274
427 Cichon, J., and Gan, W.B. (2015). Branch-specific dendritic Ca(2+) spikes cause persistent synaptic
428 plasticity. Nature *520*, 180-185. doi:10.1038/nature14251
429 Clark, B.D., Kwon, E., Maffie, J., Jeong, H.Y., Nadal, M., Strop, P., and Rudy, B. (2008). DPP6
430 Localization in Brain Supports Function as a Kv4 Channel Associated Protein. Front Mol Neurosci *1*,
431 8. doi:10.3389/neuro.02.008.2008
432 Cook, E.P., and Johnston, D. (1999). Voltage-dependent properties of dendrites that eliminate location-
433 dependent variability of synaptic input. J Neurophysiol *81*, 535-543.
434 Foeger, N.C., Norris, A.J., Wren, L.M., and Nerbonne, J.M. (2012). Augmentation of Kv4.2-encoded
435 currents by accessory dipeptidyl peptidase 6 and 10 subunits reflects selective cell surface Kv4.2
436 protein stabilization. J Biol Chem *287*, 9640-9650. doi:10.1074/jbc.M111.324574
437 Frick, A., Magee, J., Koester, H.J., Migliore, M., and Johnston, D. (2003). Normalization of Ca2+ signals
438 by small oblique dendrites of CA1 pyramidal neurons. J Neurosci *23*, 3243-3250.
439 Fukumoto, N., Kitamura, N., Niimi, K., Takahashi, E., Itakura, C., and Shibuya, I. (2012). Ca2+ channel
440 currents in dorsal root ganglion neurons of P/Q-type voltage-gated Ca2+ channel mutant mouse,
441 rolling mouse Nagoya. Neurosci Res *73*, 199-206. doi:10.1016/j.neures.2012.04.006
442 Gasparini, S. (2011). Distance- and activity-dependent modulation of spike back-propagation in layer V
443 pyramidal neurons of the medial entorhinal cortex. J Neurophysiol *105*, 1372-1379.
444 doi:10.1152/jn.00014.2010
445 Golding, N.L., Kath, W.L., and Spruston, N. (2001). Dichotomy of action-potential backpropagation in CA1
446 pyramidal neuron dendrites. J Neurophysiol *86*, 2998-3010.

447 Grewe, B.F., Bonnan, A., and Frick, A. (2010). Back-Propagation of Physiological Action Potential Output
448 in Dendrites of Slender-Tufted L5A Pyramidal Neurons. Front Cell Neurosci *4*, 13.
449 doi:10.3389/fncel.2010.00013
450 Gross, C., Yao, X., Pong, D.L., Jeromin, A., and Bassell, G.J. (2011). Fragile X mental retardation protein
451 regulates protein expression and mRNA translation of the potassium channel Kv4.2. J Neurosci *31*,
452 5693-5698. doi:10.1523/JNEUROSCI.6661-10.2011
453 Harnett, M.T., Xu, N.L., Magee, J.C., and Williams, S.R. (2013). Potassium channels control the
454 interaction between active dendritic integration compartments in layer 5 cortical pyramidal neurons.
455 Neuron *79*, 516-529. doi:10.1016/j.neuron.2013.06.005
456 Hayama, T., Noguchi, J., Watanabe, S., Takahashi, N., Hayashi-Takagi, A., Ellis-Davies, G.C., Matsuzaki,
457 M., and Kasai, H. (2013). GABA promotes the competitive selection of dendritic spines by controlling
458 local Ca2+ signaling. Nat Neurosci *16*, 1409-1416. doi:10.1038/nn.3496
459 Higley, M.J., and Contreras, D. (2006). Balanced excitation and inhibition determine spike timing during
460 frequency adaptation. J Neurosci *26*, 448-457. doi:10.1523/JNEUROSCI.3506-05.2006
461 Hoffman, D.A., Magee, J.C., Colbert, C.M., and Johnston, D. (1997). K+ channel regulation of signal
462 propagation in dendrites of hippocampal pyramidal neurons. Nature *387*, 869-875. doi:10.1038/43119
463 Jinno, S., Jeromin, A., and Kosaka, T. (2005). Postsynaptic and extrasynaptic localization of Kv4.2
464 channels in the mouse hippocampal region, with special reference to targeted clustering at gabaergic
465 synapses. Neuroscience *134*, 483-494. doi:10.1016/j.neuroscience.2005.04.065
466 Johnston, D., and Narayanan, R. (2008). Active dendrites: colorful wings of the mysterious butterflies.
467 Trends Neurosci *31*, 309-316. doi:10.1016/j.tins.2008.03.004
468 Kalmbach, B.E., Johnston, D., and Brager, D.H. (2015). Cell-Type Specific Channelopathies in the
469 Prefrontal Cortex of the fmr1-/y Mouse Model of Fragile X Syndrome. eNeuro *2*.
470 doi:10.1523/ENEURO.0114-15.2015
471 Kameyama, M., Kameyama, A., Kaibara, M., Nakayama, T., and Irisawa, H. (1989). Intracellular
472 mechanisms involved in "run-down" of calcium channels. Adv Exp Med Biol *255*, 111-117.
473 Kanemoto, Y., Matsuzaki, M., Morita, S., Hayama, T., Noguchi, J., Senda, N., Momotake, A., Arai, T., and
474 Kasai, H. (2011). Spatial distributions of GABA receptors and local inhibition of Ca2+ transients
475 studied with GABA uncaging in the dendrites of CA1 pyramidal neurons. PLoS One *6*, e22652.
476 doi:10.1371/journal.pone.0022652
477 Kim, J., Jung, S.C., Clemens, A.M., Petralia, R.S., and Hoffman, D.A. (2007). Regulation of dendritic
478 excitability by activity-dependent trafficking of the A-type K+ channel subunit Kv4.2 in hippocampal
479 neurons. Neuron *54*, 933-947. doi:10.1016/j.neuron.2007.05.026
480 Kim, J., Wei, D.S., and Hoffman, D.A. (2005). Kv4 potassium channel subunits control action potential
481 repolarization and frequency-dependent broadening in rat hippocampal CA1 pyramidal neurones. J
482 Physiol *569*, 41-57. doi:10.1113/jphysiol.2005.095042
483 Korngreen, A., and Sakmann, B. (2000). Voltage-gated K+ channels in layer 5 neocortical pyramidal
484 neurones from young rats: subtypes and gradients. J Physiol *525 Pt 3*, 621-639. doi:10.1111/j.1469-
485 7793.2000.00621.x
486 Larkum, M.E., Zhu, J.J., and Sakmann, B. (1999). A new cellular mechanism for coupling inputs arriving
487 at different cortical layers. Nature *398*, 338-341. doi:10.1038/18686
488 Losonczy, A., Makara, J.K., and Magee, J.C. (2008). Compartmentalized dendritic plasticity and input
489 feature storage in neurons. Nature *452*, 436-441. doi:10.1038/nature06725
490 Lovett-Barron, M., Turi, G.F., Kaifosh, P., Lee, P.H., Bolze, F., Sun, X.H., Nicoud, J.F., Zemelman, B.V.,
491 Sternson, S.M., and Losonczy, A. (2012). Regulation of neuronal input transformations by tunable
492 dendritic inhibition. Nat Neurosci *15*, 423-430, S421-423. doi:10.1038/nn.3024
493 Maffie, J.K., Dvoretskova, E., Bougis, P.E., Martin-Eauclaire, M.F., and Rudy, B. (2013). Dipeptidyl-
494 peptidase-like-proteins confer high sensitivity to the scorpion toxin AmmTX3 to Kv4-mediated A-type
495 K+ channels. J Physiol *591*, 2419-2427. doi:10.1113/jphysiol.2012.248831
496 Magee, J.C., and Carruth, M. (1999). Dendritic voltage-gated ion channels regulate the action potential
497 firing mode of hippocampal CA1 pyramidal neurons. J Neurophysiol *82*, 1895-1901.
498 Magee, J.C., and Johnston, D. (1997). A synaptically controlled, associative signal for Hebbian plasticity
499 in hippocampal neurons. Science *275*, 209-213. doi:10.1126/science.275.5297.209
500 Markram, H., Lubke, J., Frotscher, M., and Sakmann, B. (1997). Regulation of synaptic efficacy by
501 coincidence of postsynaptic APs and EPSPs. Science *275*, 213-215.
502 doi:10.1126/science.275.5297.213

503 Marlin, J.J., and Carter, A.G. (2014). GABA-A receptor inhibition of local calcium signaling in spines and
504 dendrites. J Neurosci *34*, 15898-15911. doi:10.1523/JNEUROSCI.0869-13.2014
505 Migliore, M., Hoffman, D.A., Magee, J.C., and Johnston, D. (1999). Role of an A-type K+ conductance in
506 the back-propagation of action potentials in the dendrites of hippocampal pyramidal neurons. J
507 Comput Neurosci *7*, 5-15.
508 Miles, R., Tóth, K., Gulyás, A.I., Hájos, N., and Freund, T.F. (1996). Differences between Somatic and
509 Dendritic Inhibition in the Hippocampus. Neuron *16*, 815-823. doi:10.1016/S0896-6273(00)80101-4
510 Miller, J.P., Rall, W., and Rinzel, J. (1985). Synaptic amplification by active membrane in dendritic spines.
511 Brain Res *325*, 325-330. doi:10.1016/0006-8993(85)90333-6
512 Mullner, F.E., Wierenga, C.J., and Bonhoeffer, T. (2015). Precision of Inhibition: Dendritic Inhibition by
513 Individual GABAergic Synapses on Hippocampal Pyramidal Cells Is Confined in Space and Time.
514 Neuron *87*, 576-589. doi:10.1016/j.neuron.2015.07.003
515 Paille, V., Fino, E., Du, K., Morera-Herreras, T., Perez, S., Kotaleski, J.H., and Venance, L. (2013).
516 GABAergic circuits control spike-timing-dependent plasticity. J Neurosci *33*, 9353-9363.
517 doi:10.1523/JNEUROSCI.5796-12.2013
518 Palmer, L., Murayama, M., and Larkum, M. (2012). Inhibitory Regulation of Dendritic Activity in vivo. Front
519 Neural Circuits *6*, 26. doi:10.3389/fncir.2012.00026
520 Pathak, D., Guan, D., and Foehring, R.C. (2016). Roles of specific Kv channel types in repolarization of
521 the action potential in genetically identified subclasses of pyramidal neurons in mouse neocortex. J
522 Neurophysiol *115*, 2317-2329. doi:10.1152/jn.01028.2015
523 Poirazi, P., and Mel, B.W. (2001). Impact of active dendrites and structural plasticity on the memory
524 capacity of neural tissue. Neuron *29*, 779-796. doi:10.1016/S0896-6273(01)00252-5
525 Pouille, F., and Scanziani, M. (2001). Enforcement of temporal fidelity in pyramidal cells by somatic feed-
526 forward inhibition. Science *293*, 1159-1163. doi:10.1126/science.1060342
527 Ramakers, G.M., and Storm, J.F. (2002). A postsynaptic transient K(+) current modulated by arachidonic
528 acid regulates synaptic integration and threshold for LTP induction in hippocampal pyramidal cells.
529 Proc Natl Acad Sci U S A *99*, 10144-10149. doi:10.1073/pnas.152620399
530 Rial Verde, E.M., Zayat, L., Etchenique, R., and Yuste, R. (2008). Photorelease of GABA with Visible
531 Light Using an Inorganic Caging Group. Front Neural Circuits *2*, 2. doi:10.3389/neuro.04.002.2008
532 Sandler, M., Shulman, Y., and Schiller, J. (2016). A Novel Form of Local Plasticity in Tuft Dendrites of
533 Neocortical Somatosensory Layer 5 Pyramidal Neurons. Neuron *90*, 1028-1042.
534 doi:10.1016/j.neuron.2016.04.032
535 Serodio, P., Kentros, C., and Rudy, B. (1994). Identification of molecular components of A-type channels
536 activating at subthreshold potentials. J Neurophysiol *72*, 1516-1529.
537 Serodio, P., and Rudy, B. (1998). Differential expression of Kv4 K+ channel subunits mediating
538 subthreshold transient K+ (A-type) currents in rat brain. J Neurophysiol *79*, 1081-1091.
539 Shepherd, G.M., Brayton, R.K., Miller, J.P., Segev, I., Rinzel, J., and Rall, W. (1985). Signal
540 enhancement in distal cortical dendrites by means of interactions between active dendritic spines.
541 Proc Natl Acad Sci U S A *82*, 2192-2195.
542 Stokes, C.C., Teeter, C.M., and Isaacson, J.S. (2014). Single dendrite-targeting interneurons generate
543 branch-specific inhibition. Front Neural Circuits *8*, 139. doi:10.3389/fncir.2014.00139
544 Stuart, G., Schiller, J., and Sakmann, B. (1997). Action potential initiation and propagation in rat
545 neocortical pyramidal neurons. J Physiol *505 (Pt 3)*, 617-632.
546 Tsubokawa, H., and Ross, W.N. (1996). IPSPs modulate spike backpropagation and associated [Ca2+]i
547 changes in the dendrites of hippocampal CA1 pyramidal neurons. J Neurophysiol *76*, 2896-2906.
548 Wehr, M., and Zador, A.M. (2003). Balanced inhibition underlies tuning and sharpens spike timing in
549 auditory cortex. Nature *426*, 442-446. doi:10.1038/nature02116
550 Wilmes, K.A., Sprekeler, H., and Schreiber, S. (2016). Inhibition as a Binary Switch for Excitatory
551 Plasticity in Pyramidal Neurons. PLoS Comput Biol *12*, e1004768. doi:10.1371/journal.pcbi.1004768
552 Yuste, R. (1997). Potassium channels. Dendritic shock absorbers. Nature *387*, 851, 853.
553 doi:10.1038/43063
554 Zhu, Y., Stornetta, R.L., and Zhu, J.J. (2004). Chandelier cells control excessive cortical excitation:
555 characteristics of whisker-evoked synaptic responses of layer 2/3 nonpyramidal and pyramidal
556 neurons. J Neurosci *24*, 5101-5108. doi:10.1523/JNEUROSCI.0544-04.2004

557

561 **Figure Legends**

562

563 **Figure 1. GABAergic inhibition of ΔCa2+ is enhanced by blockade of KA channels.**

564 (**A**) Whole Cell patch recording where performed in L5PNs of visual cortex. Ca2+ imaging and GABA
565 uncaging were performed along the proximal apical dendrite, as shown in the example cell (A1) and
566 schematic (A2). Scale bar 25 μm. (**B**) Example spine-dendrite pair and the associated line-scanned
567 response to a bAP. (**C**) Average ± SEM somatic voltage recorded before (black) and after (green)
568 treatment with 4-AP for action potentials (upper traces) and uncaging-evoked IPSPs. (**D**) Example bAP-
569 evoked ΔCa2+ for the apical dendritic region shown in (B) for bAP alone (black, blue) or paired with
570 GABA uncaging (red, orange) for the spine and neighboring dendrite, before (left) and after (right)
571 treatment with 5 mM 4-AP. (**E**) Average (n=10) ΔCa2+ for the population of imaged spines and dendrites,
572 colors as in (D). (**F-G**) Population data (n=10) showing the magnitude of ΔCa2+ inhibition and peak bAP-
573 evoked ΔCa2+ for spines (F) and neighboring dendrites (G) before (black) and after (green) treatment
574 with 5 mM 4-AP (Wilcoxon matched-pairs signed rank test, *p<0.05).

575

576 **Figure 1 — figure supplement 1. Picrotoxin blocks the effects of GABA uncaging.**

577 **Figure 1 — figure supplement 2. Saline does not alter GABAergic inhibition of ΔCa2+.**

578 **Figure 1 — figure supplement 3. Somatic IPSPs are enhanced by blockade of KA channels.**

579 **Figure 1 — figure supplement 4. GABAergic inhibition of ΔCa2+ is not enhanced by 4-AP in basal**
580 **dendrites**

581

582 **Figure 1— figure supplement 1. Picrotoxin blocks the effects of GABA uncaging.**

583 (**A**) Schematic of recording and imaging configuration. Experiments are performed in the presence of
584 picrotoxin (100 μM). (**B**) Average ± SEM (n=6) Ca2+ transients in proximal apical dendrites for bAP alone
585 or paired with GABA uncaging before (left) and after (right) treatment with 4-AP (colors as in Fig. 1). (**C-D**)
586 Population data (n=6) showing the magnitude of Ca2+ inhibition and peak bAP-evoked Ca2+ for spines
587 (C) and neighboring dendritic shafts (D) in control (black) and 4-AP (green) conditions (Wilcoxon
588 matched-pairs signed rank test, *p<0.05).

589

590 **Figure 1 — figure supplement 2. Saline does not alter GABAergic inhibition of ΔCa2+.**

591 (**A**) Schematic of recording and imaging configuration. (**B**) Average ± SEM (n=7) Ca2+ transients in
592 proximal apical dendrites for bAP alone or paired with GABA uncaging before (left) and after (right)
593 treatment with control saline (colors as in Fig. 1). (**C-D**) Population data (n=7) showing the magnitude of
594 Ca2+ inhibition and peak bAP-evoked Ca2+ for spines (C) and neighboring dendritic shafts (D) in control
595 (black) and saline (green) conditions (Wilcoxon matched-pairs signed rank test, *p<0.05).

596

597 **Figure 1 — figure supplement 3. Somatic IPSPs are enhanced by blockade of KA channels.**

598 (**A**) Schematic of recording configuration. (**B**) Average ± SEM (n=9) IPSPs before (black) and after
599 (green) treatment with 5 mM 4-AP for single (left) and triple (right) GABA uncaging events. (**C**) Population
600 data (n=9) showing peak IPSP amplitude (left) and ratio of third:first amplitude (right) in control (black)
601 and 4-AP (green) conditions (Wilcoxon matched-pairs signed rank test, *p<0.05). (**D**) Population data
602 (n=9) showing decay time constant for single IPSPs (Wilcoxon matched-pairs signed rank test, *p<0.05).
603 (**E**) Population data (n=9) showing somatic input resistance (Wilcoxon matched-pairs signed rank test,
604 p>0.05)
605
606 **Figure 1 — figure supplement 4. GABAergic inhibition of ΔCa2+ is not enhanced by 4-AP in basal**
607 **dendrites**
608 (**A**) Schematic of recording and imaging configuration. (**B**) Average ± SEM (n=10) Ca2+ transients in
609 basal dendrites for bAP alone or paired with GABA uncaging before (left) and after (right) treatment with
610 4-AP (colors as in Fig. 1). (**C-D**) Population data (n=10) showing the magnitude of Ca2+ inhibition and
611 peak bAP-evoked Ca2+ for spines (C) and neighboring dendritic shafts (D) in control (black) and 4-AP
612 (green) conditions (Wilcoxon matched-pairs signed rank test, *p<0.05).
613
614 **Figure 2. GABAergic inhibition of ΔCa2+ is enhanced by local blockade of KA channels.**
615 (**A**) Schematic of recording and imaging configuration, illustrating location of puffed 4-AP. (**B**) Average ±
616 SEM (n=7) Ca2+ transients for bAP alone or paired with GABA uncaging before (left) and after (right)
617 application of 4-AP to the proximal apical dendrite (colors as in Fig. 1). (**C-D**) Population data (n=7)
618 showing the magnitude of Ca2+ inhibition and peak bAP-evoked Ca2+ for spines (C) and neighboring
619 dendritic shafts (D) in control (black) and 4-AP (green) conditions (Wilcoxon matched-pairs signed rank
620 test, *p<0.05).
621 **Figure 2 — figure supplement 1. GABAergic inhibition of ΔCa2+ in the proximal apical dendrite is**
622 **not affected by somatic or distal dendritic KA channel blockade.**
623 **Figure 2 — figure supplement 2. Effect of blockade of potassium channels at proximal apical**
624 **dendrite and soma on somatic IPSP.**
625
626 **Figure 2 — figure supplement 1. GABAergic inhibition of ΔCa2+ in the proximal apical dendrite is**
627 **not affected by somatic or distal dendritic KA channel blockade.**
628 (**A**) Schematic of recording and imaging configuration, illustrating somatic location of puffed 4-AP. (**B**)
629 Average ± SEM (n=6) Ca2+ transients for bAP alone or paired with GABA uncaging before (left) and after
630 (right) application of 4-AP to the soma (colors as in Fig. 1). (**C-D**) Population data (n=6) showing the
631 magnitude of Ca2+ inhibition and peak bAP-evoked Ca2+ for spines (C) and neighboring dendritic shafts
632 (D) in control (black) and 4-AP (green) conditions (Wilcoxon matched-pairs signed rank test, p>0.05). (**E**)
633 Schematic of experimental configuration, illustrating distal dendritic location of puffed 4-AP. (**F**) Average ±
634 SEM (n=6) Ca2+ transients for bAP alone of paired with GABA uncaging before (left) and after (right)

application of 4-AP to the distal dendrite (colors as in Fig. 1). (**G-H**) Population data (n=6) showing the magnitude of Ca2+ inhibition and peak bAP-evoked Ca2+ for spines (G) and neighboring dendritic shafts (H) in control (black) and 4-AP (green) conditions (Wilcoxon matched-pairs signed rank test, p>0.05).

Figure 2 — figure supplement 2. Effect of blockade of potassium channels at proximal apical dendrite and soma on somatic IPSP

(**A**) Schematic of recording configuration, illustrating dendritic location of puffed 4-AP. (**B**) Average ± SEM (n=9) IPSPs before (black) and after (green) application of 4-AP to the apical dendrite for single (upper) and triple (lower) GABA uncaging events. (**C**) Population data (n=9) showing peak IPSP amplitude (left) and ratio of third:first amplitude (right)(Wilcoxon matched-pairs signed rank test, *p<0.05). (**D**) Population data (n=9) showing decay time constant for single IPSPs (Wilcoxon matched-pairs signed rank test, p<0.05). (**E**) Population data (n=9) showing somatic input resistance (Wilcoxon matched-pairs signed rank test, p<0.05). (**F-J**) As in (A-E) for local application of 4-AP to the soma (n=9, Wilcoxon matched-pairs signed rank test, *p<0.05).

Figure 3. GABAergic inhibition of ΔCa2+ is enhanced by blockade of Kv4 channels using AmmTx3.

(**A**) Schematic showing recording and imaging configuration. (**B**) Average ± SEM (n=10) Ca2+ transients for bAP alone or paired with GABA uncaging, before (left) and after (right) treatment with the selective Kv4 blocker AmmTx3 (200 nM) (colors as in Fig. 1). (**C-D**) Population data (n=10) showing the magnitude of Ca2+ inhibition and peak bAP-evoked Ca2+ for spines (C) and neighboring dendritic shafts (D) in control (black) and AmmTx3 (green) conditions (Wilcoxon matched-pairs signed rank test, *p<0.05).

Figure 3 — figure supplement 1. Blockade of Kv4 by AmmTx3 has no effect on somatic IPSP

Figure 3 — figure supplement 2. Outside-out recordings reveal expression of Kv4 channels.

Figure 3 — figure supplement 1. Blockade of Kv4 by AmmTx3 has no effect on somatic IPSP

(**A**) Schematic of recording configuration. (**B**) Average ± SEM (n=6) IPSPs before (black) and after (green) treatment with 200 nM AmmTx3 for single (left) and triple (right) GABA uncaging events. (**C**) Population data (n=6) showing peak IPSP amplitude (left) and ratio of third:first amplitude (right) in control (black) and AmmTx3 (green) conditions (Wilcoxon matched-pairs signed rank test, *p<0.05). (**D**) Population data (n=6) showing decay time constant for single IPSPs (Wilcoxon matched-pairs signed rank test, p>0.05). (**E**) Population data (n=6) showing somatic input resistance (Wilcoxon matched-pairs signed rank test, *p>0.05).

Figure 3 — figure supplement 2. Outside-out recordings reveal expression of Kv4 channels.

(**A**) Peak-normalized average ± SEM (n=6) currents evoked in somatic outside-out patches before (black) and after (green) treatment with 4-AP. (**B**) Peak-normalized average ± SEM (n=6) currents evoked in

outside-out patches before (black) and after (green) treatment with AmmTx3. (**C**) Population data (n=6) showing reduction in current produced by 4-AP or AmmTx3 for the measured intervals marked in (A)(Wilcoxon matched-pairs signed rank test for single columns, Unpaired t-test for comparison between treatments, *p<0.05).

Figure 4. Somatic activity enhances GABAergic inhibition of dendritic ΔCa2+.

(**A**) Average ± SEM (n=10) of somatic recordings for a single action potential (black) or when preceded 20 ms by a 100 Hz train of action potentials (green). Inset shows change in spike waveform. (**B**) Average ± SEM (n=10) Ca2+ transients for bAP alone or paired with GABA uncaging, presented either singly (left) or following a 100 Hz train of action potentials (right)(colors as in Fig. 1). (**C-D**) Population data (n=10) showing the magnitude of Ca2+ inhibition and peak bAP-evoked Ca2+ for spines (C) and neighboring dendritic shafts (D), presented either singly (black) or following a 100 Hz train of action potentials (green)(Wilcoxon matched-pairs signed rank test, *p<0.05).

Figure 4— figure supplement1. Activity-dependent enhancement of GABAergic inhibition is frequency-dependent and occluded by blockade of KA channels.

Figure 4— figure supplement1. Activity-dependent enhancement of GABAergic inhibition is frequency-dependent and occluded by blockade of KA channels.

(**A**) Average ± SEM (n=10) of somatic recordings for a single action potential (black) or when preceded 20 ms by a 50 Hz train of action potentials (green). Inset shows change in spike waveform. (**B**) Average ± SEM (n=10) Ca2+ transients for bAP alone or paired with GABA uncaging, presented either singly (left) or following a 50 Hz train of action potentials (right)(colors as in Fig. 1). (**C-D**) Population data (n=10) showing the magnitude of Ca2+ inhibition and peak bAP-evoked Ca2+ for spines (C) and neighboring dendritic shafts (D), presented either single (black) or following a 50 Hz train of action potentials (green)(Wilcoxon matched-pairs signed rank test, *p<0.05). (**E**) Average ± SEM (n=10) of somatic recordings for a single action potential (black) or when preceded 20 ms by a 100 Hz train of action potentials (green), in the presence of 5 mM 4-AP. (**F-H**) As in (B-D) for a 100 Hz preceding train and in the presence of 5 mM 4-AP (n=10, Wilcoxon matched-pairs signed rank test, *p<0.05).

Figure 5. Somatic activity enhances synaptic GABAergic inhibition of ΔCa2+.

(**A**) Schematic showing recording and imaging configuration. ChR2 was virally expressed in somatostatin-containing interneurons (SOM-INs) and activated with blue light pulses. (**B**) Average ± SEM (n=10) Ca2+ transients for bAP alone or paired with optical stimulation of SOM-INs, presented either singly (left) or following a 100 Hz train of action potentials (right)(colors as in Fig. 1). (**C-D**) Population data (n=10) showing the magnitude of Ca2+ inhibition and peak bAP-evoked Ca2+ for spines (C) and neighboring dendritic shafts (D), presented either singly (black) or following a 100 Hz train of action potentials (green)(Wilcoxon matched-pairs signed rank test, *p<0.05).

709 **Figure 6. Computational simulations reveal mechanisms underlying KA-dependent regulation of**
710 **inhibition.**
711 (**A**) Simulated Ca2+ currents under three different conditions (indicated in figure) for bAPs evoked alone
712 (black) or preceded by GABAergic inhibition (red). Yellow shading indicates integral of inhibited Ca2+. (**B**)
713 Relationship between sodium reversal potential and either peak membrane potential (left) or Ca2+
714 inhibition (right). For peak V_m data, values for bAP alone (black), bAP paired with inhibition (red), and
715 resting V_m (green) are shown. (**C**) Relationship between KA conductance and either peak membrane
716 potential (left) or Ca2+ inhibition (right). Colors are as in (B). (**D**) Relationship between peak V_m and Ca2+
717 inhibition under conditions where either sodium reversal potential (closed circles) or KA conductance
718 (open circles) was varied. (**E**) Relationship between action potential duration and Ca2+ inhibition under
719 conditions where either sodium reversal potential (closed circles) or KA conductance (open circles) was
720 varied.
721
722

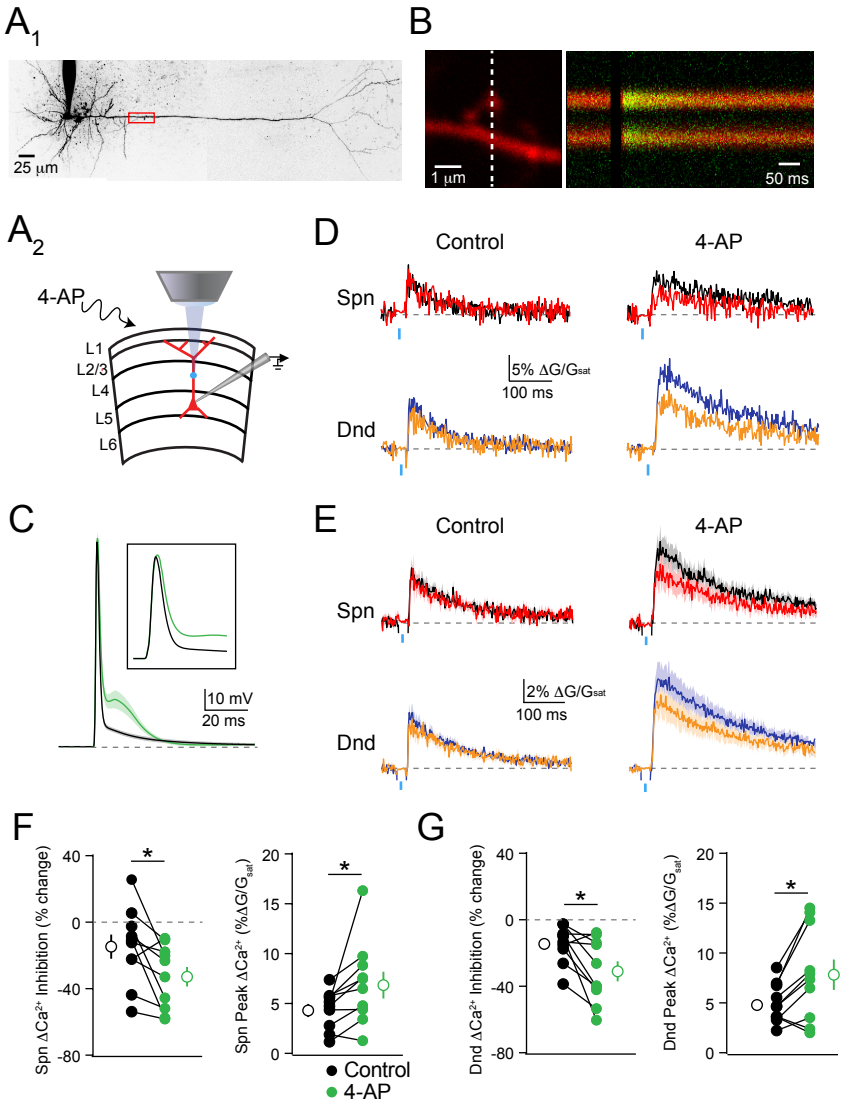
A1
25 μm
B
1 μm
50 ms
A2
4-AP
L1
L2/3
L4
L5
L6
D
Control
4-AP
Spn
Dnd
5% ΔG/Gsat
100 ms
C
10 mV
20 ms
E
Control
4-AP
Spn
Dnd
2% ΔG/Gsat
100 ms
F
Spn ΔCa2+ Inhibition (% change)
Spn Peak ΔCa2+ (%ΔG/Gsat)
Control
4-AP
G
Dnd ΔCa2+ Inhibition (% change)
Dnd Peak ΔCa2+ (%ΔG/Gsat)

Figure 1

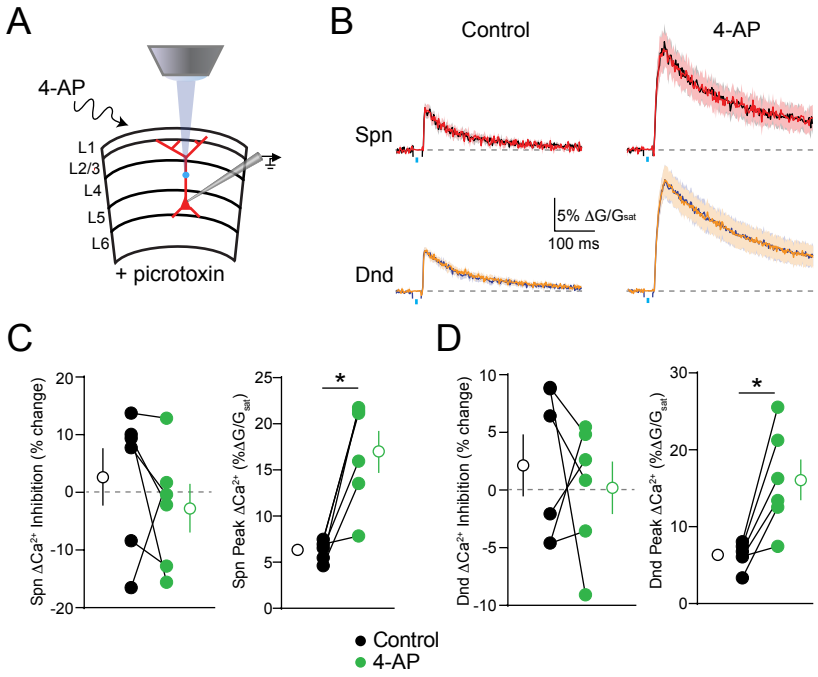
A
4-AP
L1
L2/3
L4
L5
L6
+ picrotoxin
B
Control
4-AP
Spn
Dnd
5% ΔG/Gsat
100 ms
C
Spn ΔCa2+ Inhibition (% change)
Spn Peak ΔCa2+ (%ΔG/Gsat)
*
D
Dnd ΔCa2+ Inhibition (% change)
Dnd Peak ΔCa2+ (%ΔG/Gsat)
*
Control
4-AP

Figure 1 S1

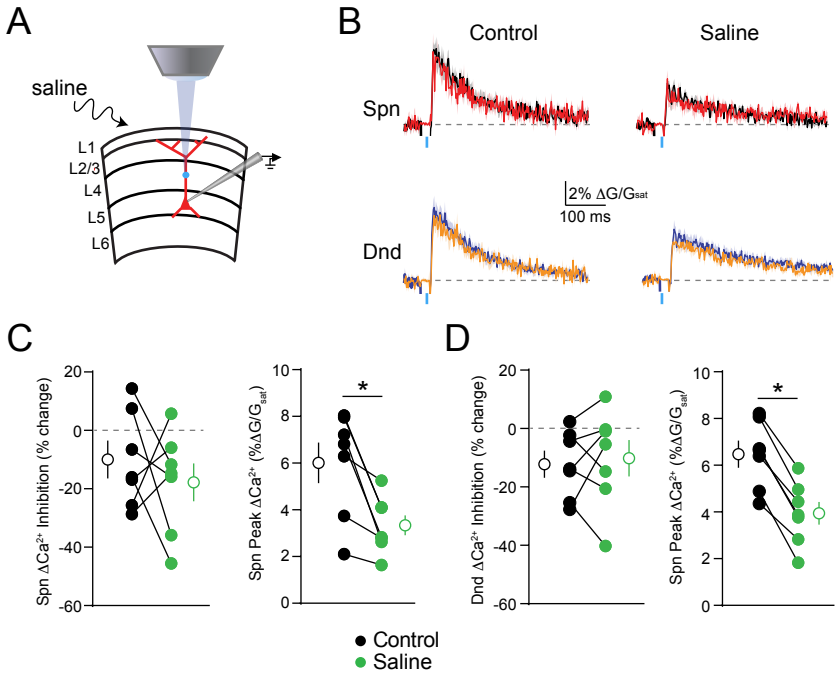
A
saline
L1
L2/3
L4
L5
L6
B
Control
Saline
Spn
Dnd
2% ΔG/Gsat
100 ms
C
D
Spn ΔCa2+ Inhibition (% change)
Spn Peak ΔCa2+ (%ΔG/Gsat)
Dnd ΔCa2+ Inhibition (% change)
Control
Saline

Figure 1 S2

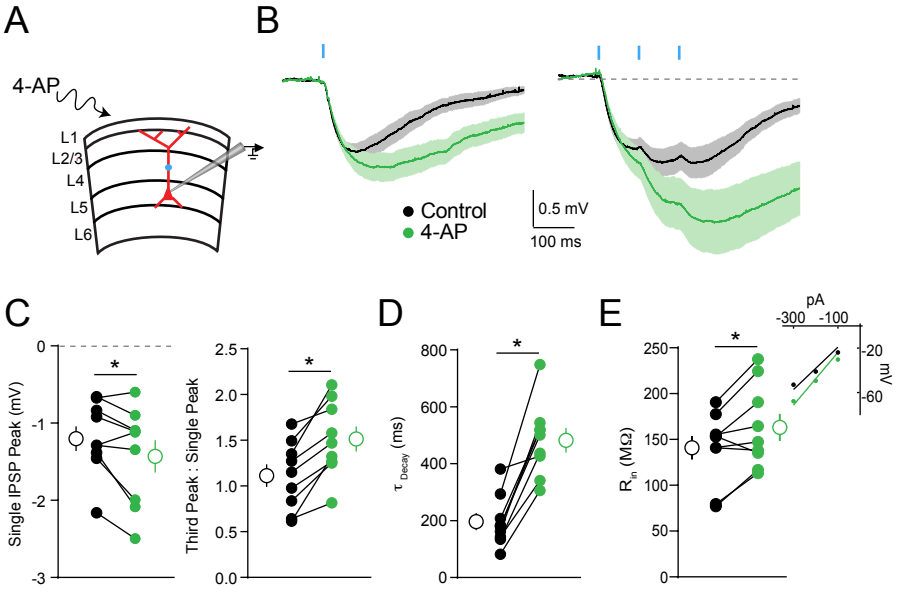
A
4-AP
L1
L2/3
L4
L5
L6
B
Control
4-AP
0.5 mV
100 ms
C
Single IPSP Peak (mV)
Third Peak : Single Peak
D
τ Decay (ms)
E
pA
-300
-100
mV
-20
-60
Rin (MΩ)

Figure 1 S3

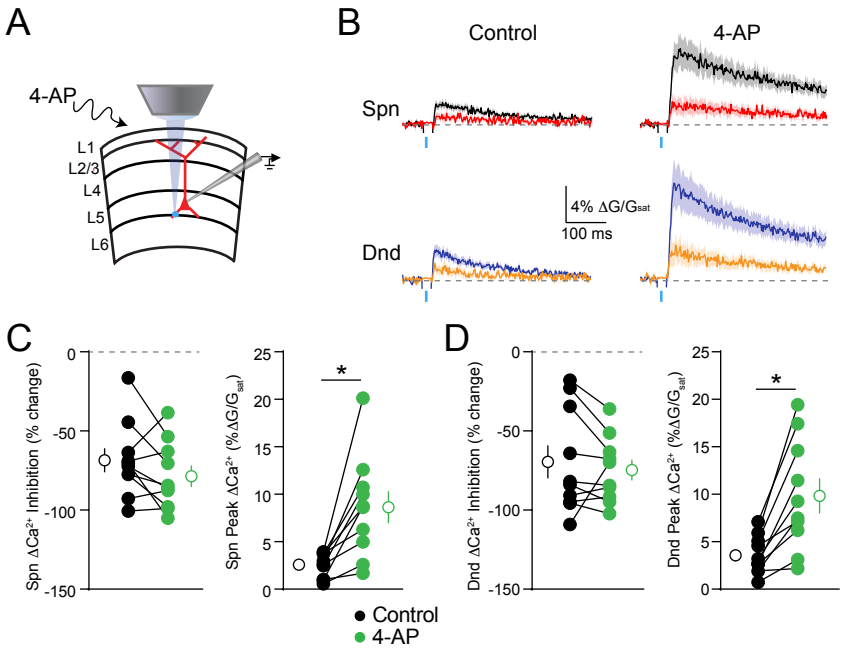
A
4-AP
L1
L2/3
L4
L5
L6
B
Control
4-AP
Spn
Dnd
4% ΔG/Gsat
100 ms
C
Spn ΔCa2+ Inhibition (% change)
Spn Peak ΔCa2+ (%ΔG/Gsat)
D
Dnd ΔCa2+ Inhibition (% change)
Dnd Peak ΔCa2+ (%ΔG/Gsat)
Control
4-AP

Figure 1 S4

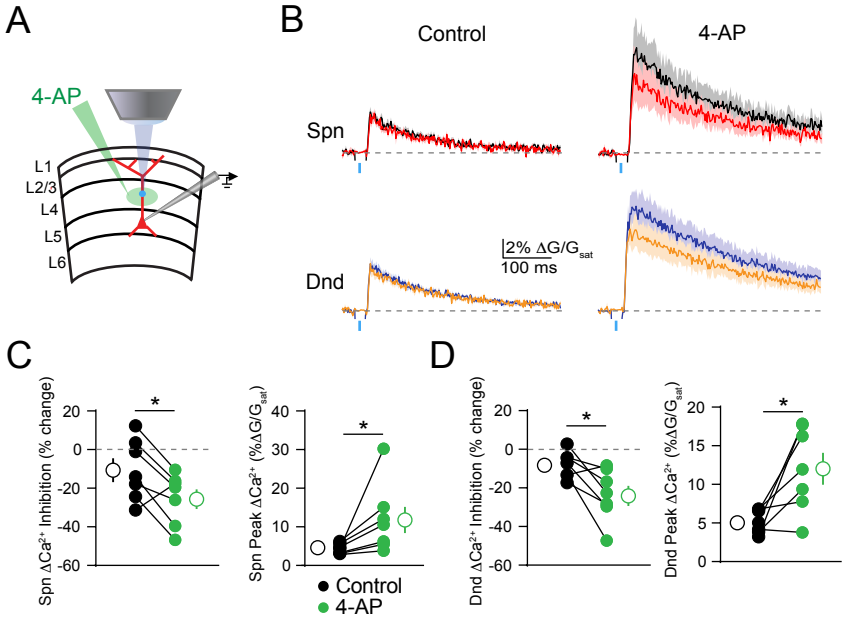
A
4-AP
L1
L2/3
L4
L5
L6
B
Control
4-AP
Spn
Dnd
2% ΔG/G_sat
100 ms
C
Spn ΔCa2+ Inhibition (% change)
Spn Peak ΔCa2+ (%ΔG/G_sat)
Control
4-AP
D
Dnd ΔCa2+ Inhibition (% change)
Dnd Peak ΔCa2+ (%ΔG/G_sat)

Figure 2

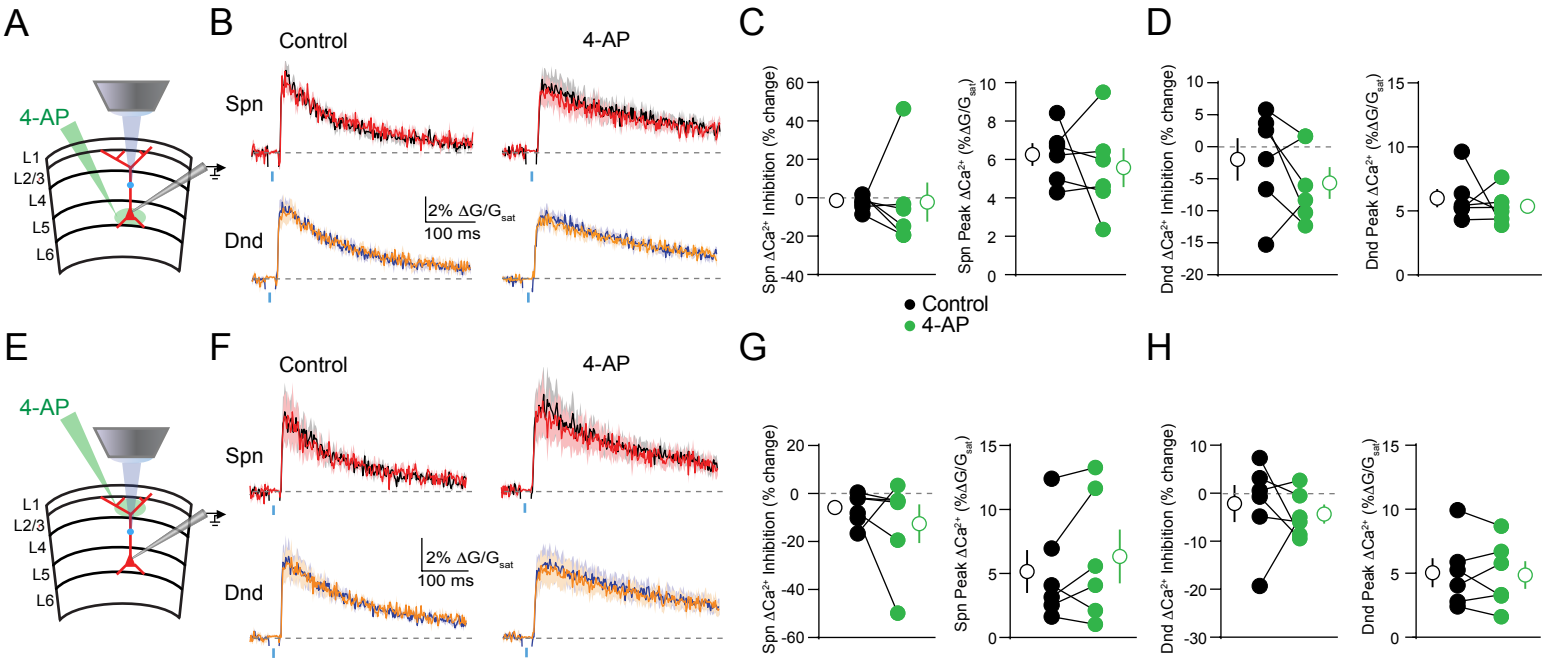
A
4-AP
L1
L2/3
L4
L5
L6
B
Control
4-AP
Spn
Dnd
2% ΔG/G$_{sat}$
100 ms
C
Spn ΔCa^{2+} Inhibition (% change)
Spn Peak ΔCa^{2+} (%ΔG/G$_{sat}$)
Control
4-AP
D
Dnd ΔCa^{2+} Inhibition (% change)
Dnd Peak ΔCa^{2+} (%ΔG/G$_{sat}$)
E
4-AP
L1
L2/3
L4
L5
L6
F
Control
4-AP
Spn
Dnd
2% ΔG/G$_{sat}$
100 ms
G
Spn ΔCa^{2+} Inhibition (% change)
Spn Peak ΔCa^{2+} (%ΔG/G$_{sat}$)
H
Dnd ΔCa^{2+} Inhibition (% change)
Dnd Peak ΔCa^{2+} (%ΔG/G$_{sat}$)

Figure 2 S1

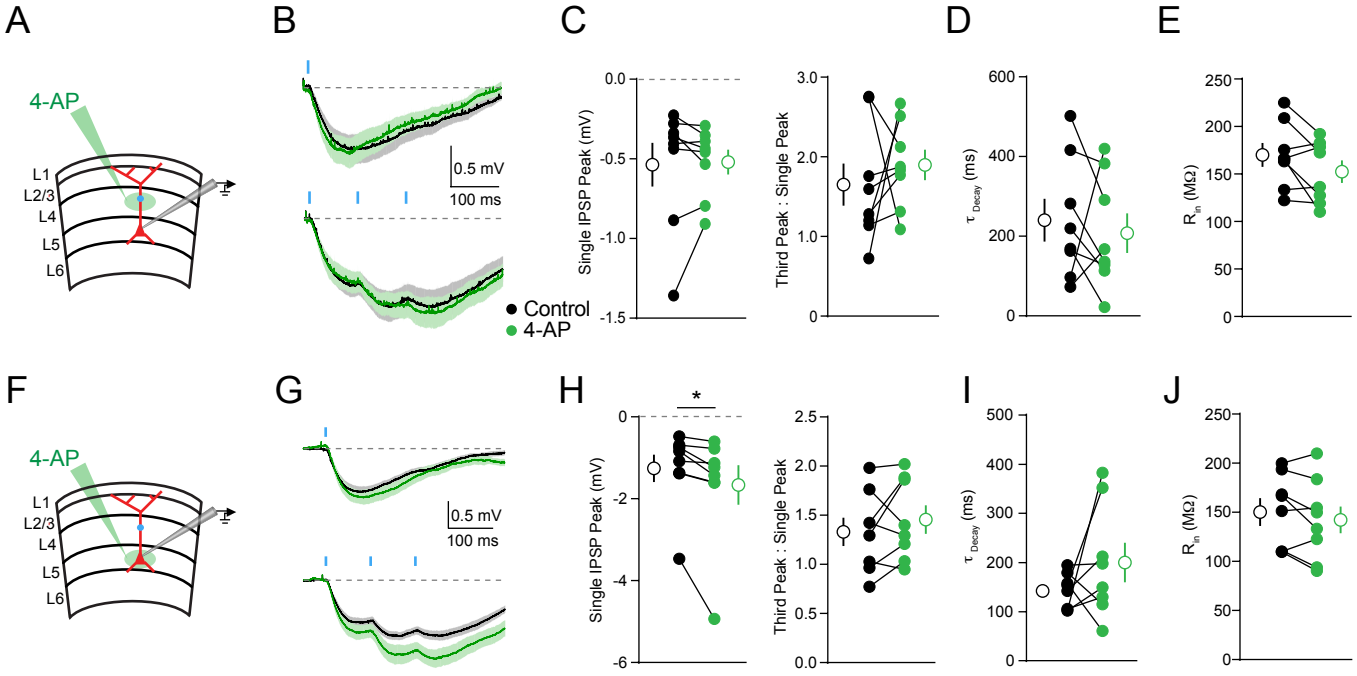
A
B
C
D
E
4-AP
L1
L2/3
L4
L5
L6
0.5 mV
100 ms
Control
4-AP
Single IPSP Peak (mV)
Third Peak : Single Peak
τ Decay (ms)
R in (MΩ)
F
G
H
I
J
*

Figure 2 S2

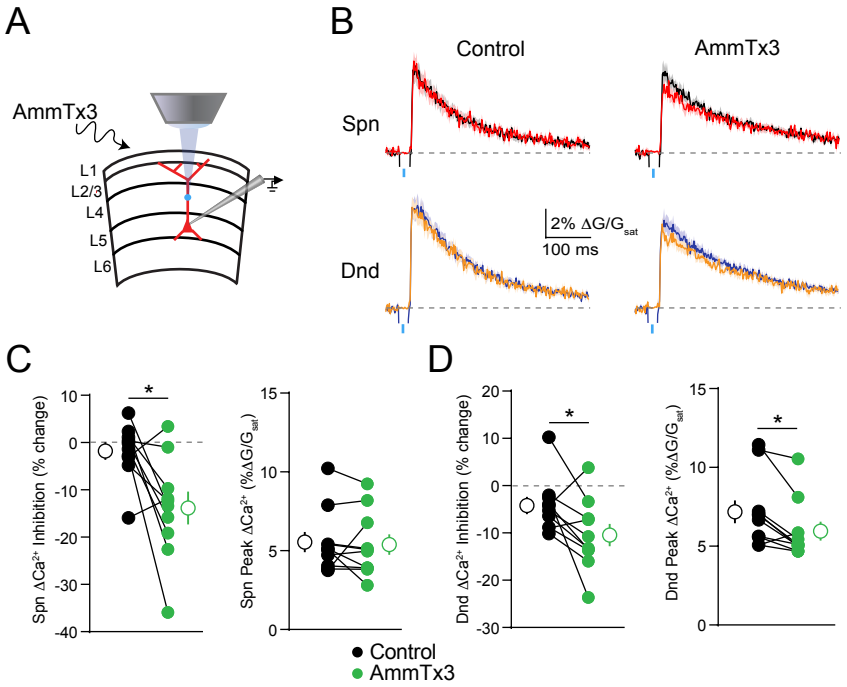
A
AmmTx3
L1
L2/3
L4
L5
L6
B
Control
AmmTx3
Spn
Dnd
2% ΔG/G_sat
100 ms
C
Spn ΔCa2+ Inhibition (% change)
Spn Peak ΔCa2+ (%ΔG/G_sat)
D
Dnd ΔCa2+ Inhibition (% change)
Dnd Peak ΔCa2+ (%ΔG/G_sat)
Control
AmmTx3

Figure 3

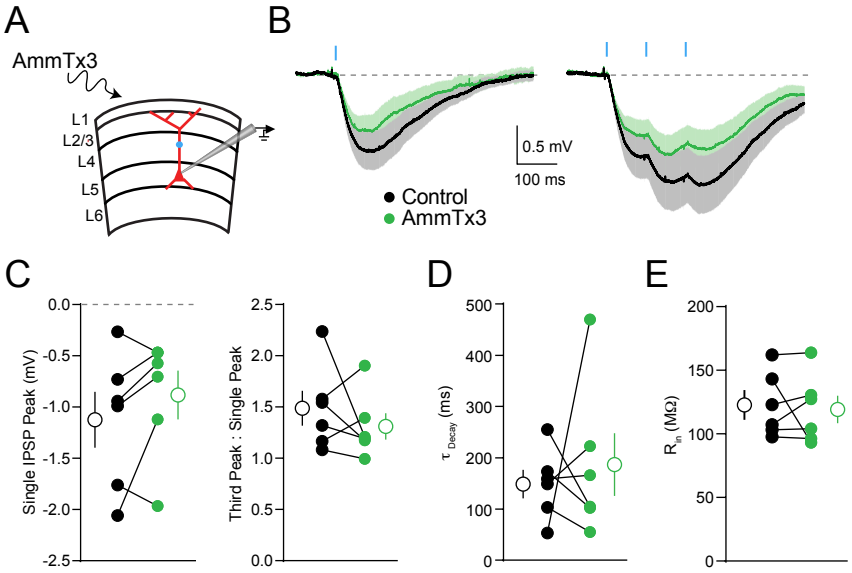
A
AmmTx3
L1
L2/3
L4
L5
L6
B
0.5 mV
100 ms
Control
AmmTx3
C
Single IPSP Peak (mV)
Third Peak : Single Peak
D
τ Decay (ms)
E
Rin (MΩ)

Figure 3 S1

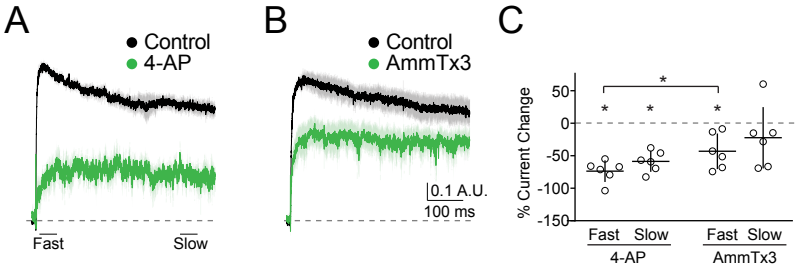
A
Control
4-AP
Fast
Slow
B
Control
AmmTx3
0.1 A.U.
100 ms
C
% Current Change
50
0
-50
-100
-150
Fast
Slow
4-AP
Fast
Slow
AmmTx3

Figure 3 S2

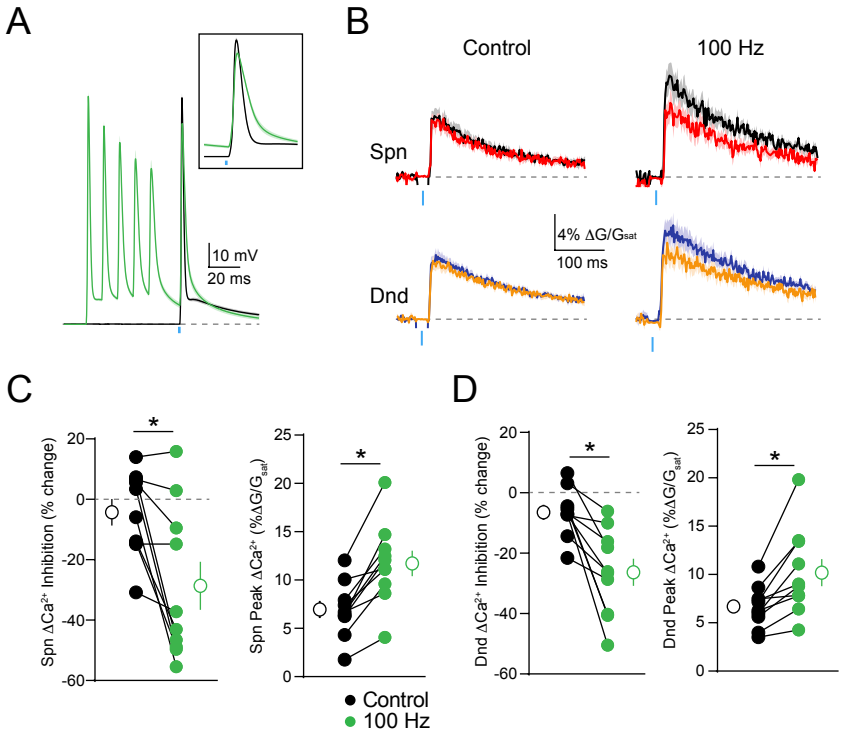
A
10 mV
20 ms
B
Control
100 Hz
Spn
Dnd
4% ΔG/Gsat
100 ms
C
D
Spn ΔCa2+ Inhibition (% change)
Spn Peak ΔCa2+ (%ΔG/Gsat)
Dnd ΔCa2+ Inhibition (% change)
Dnd Peak ΔCa2+ (%ΔG/Gsat)
Control
100 Hz

Figure 4

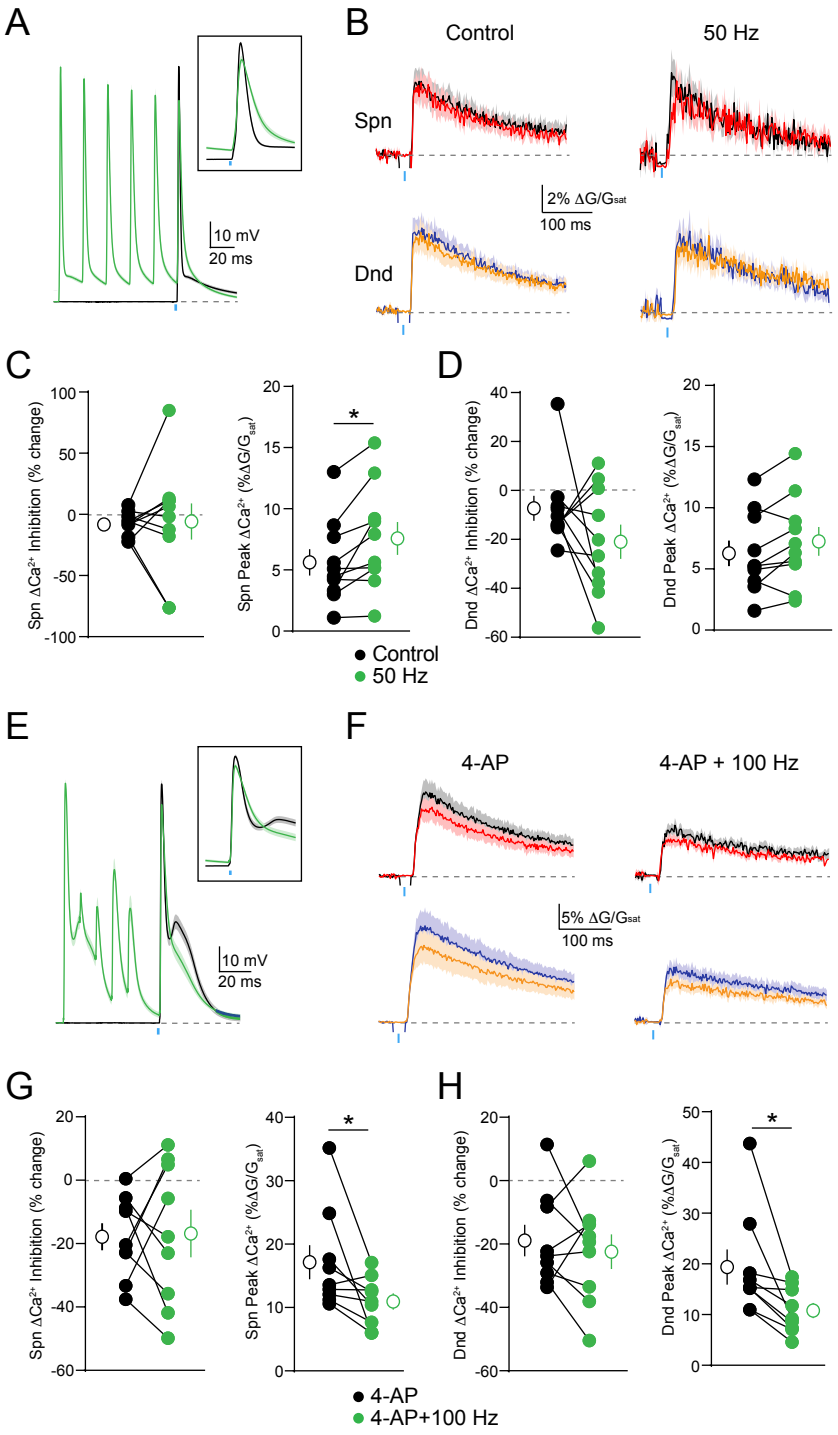
A
10 mV
20 ms
B
Control
50 Hz
Spn
Dnd
2% ΔG/Gsat
100 ms
C
Spn ΔCa2+ Inhibition (% change)
Spn Peak ΔCa2+ (%ΔG/Gsat)
*
D
Dnd ΔCa2+ Inhibition (% change)
Dnd Peak ΔCa2+ (%ΔG/Gsat)
Control
50 Hz
E
10 mV
20 ms
F
4-AP
4-AP + 100 Hz
5% ΔG/Gsat
100 ms
G
Spn ΔCa2+ Inhibition (% change)
Spn Peak ΔCa2+ (%ΔG/Gsat)
*
H
Dnd ΔCa2+ Inhibition (% change)
Dnd Peak ΔCa2+ (%ΔG/Gsat)
*
4-AP
4-AP+100 Hz

Figure 4 S1

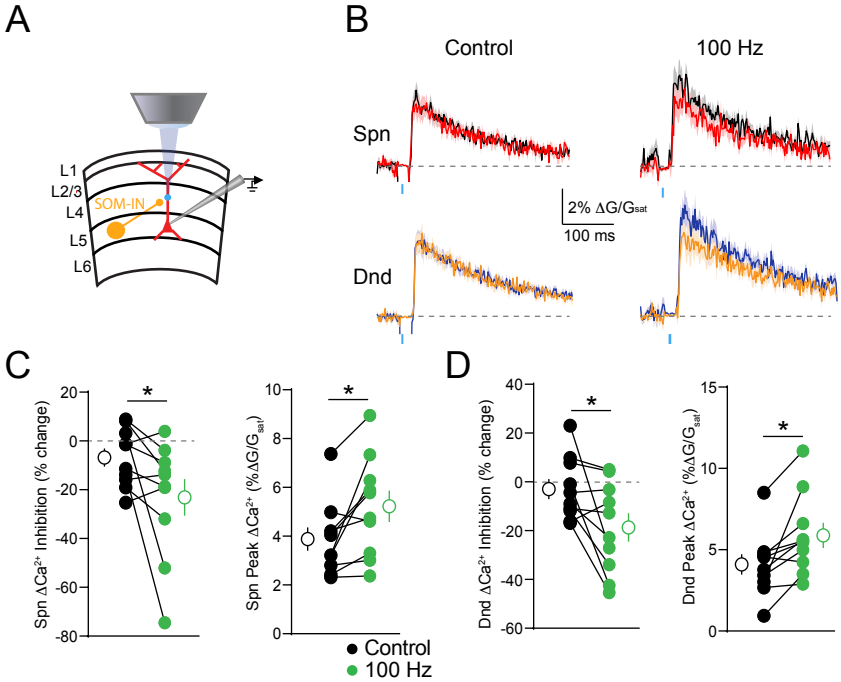
A
B
Control
100 Hz
Spn
Dnd
L1
L2/3
L4
L5
L6
SOM-IN
2% ΔG/Gsat
100 ms
C
D
Spn ΔCa2+ Inhibition (% change)
Spn Peak ΔCa2+ (%ΔG/Gsat)
Dnd ΔCa2+ Inhibition (% change)
Dnd Peak ΔCa2+ (%ΔG/Gsat)
Control
100 Hz

Figure 5

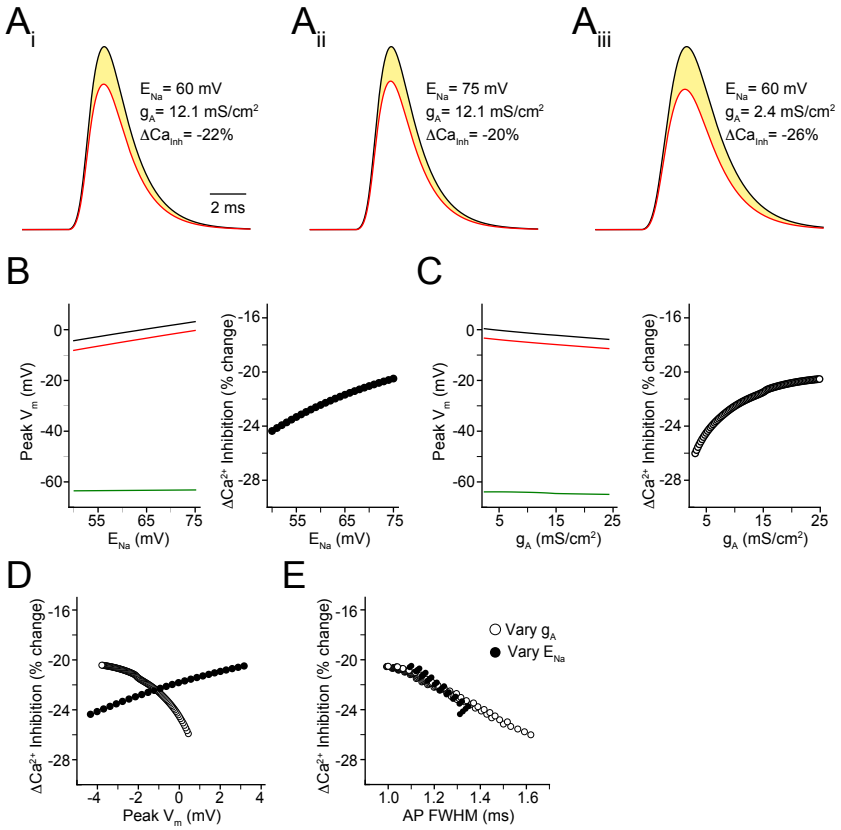
A_i
E_Na = 60 mV
g_A = 12.1 mS/cm²
ΔCa_Inh = -22%
2 ms
A_ii
E_Na = 75 mV
g_A = 12.1 mS/cm²
ΔCa_Inh = -20%
A_iii
E_Na = 60 mV
g_A = 2.4 mS/cm²
ΔCa_Inh = -26%
B
Peak V_m (mV)
E_Na (mV)
ΔCa²⁺ Inhibition (% change)
C
g_A (mS/cm²)
D
Peak V_m (mV)
E
AP FWHM (ms)
Vary g_A
Vary E_Na

Figure 6